Title
Efficiency of Launching Highly Confined Polaritons by Infrared Light Incident on a Hyperbolic Material

Journal
Nano Letters, 17(9)

ISSN
1530-6984

Authors
Dai, Siyuan
Ma, Qiong
Yang, Yafang
et al.

Publication Date
2017-09-13

DOI
10.1021/acs.nanolett.7b01587

Peer reviewed

Efficiency of Launching Highly Confined Polaritons by Infrared Light Incident on a Hyperbolic Material

Article *in* Nano Letters · August 2017

DOI: 10.1021/acs.nanolett.7b01587

18 authors, including:

Siyuan Dai
University of California, San Diego
32 PUBLICATIONS **847** CITATIONS
SEE PROFILE

Yafang Yang
Massachusetts Institute of Technology
12 PUBLICATIONS **920** CITATIONS
SEE PROFILE

Jeremy Rosenfeld
University of California, San Diego
3 PUBLICATIONS **8** CITATIONS
SEE PROFILE

Alexander S McLeod
Columbia University
74 PUBLICATIONS **2,119** CITATIONS
SEE PROFILE

NANO LETTERS

Letter

pubs.acs.org/NanoLett

Efficiency of Launching Highly Confined Polaritons by Infrared Light Incident on a Hyperbolic Material

Siyuan Dai,[†] Qiong Ma,[‡] Yafang Yang,[‡] Jeremy Rosenfeld,[†] Michael D. Goldflam,[†] Alex McLeod,[†] Zhiyuan Sun,[†] Trond I. Andersen,[‡] Zhe Fei,[†] Mengkun Liu,[†] Yinming Shao,[†] Kenji Watanabe,[§] Takashi Taniguchi,[§] Mark Thiemens,[‖] Fritz Keilmann,[⊥] Pablo Jarillo-Herrero,[‡] Michael M. Fogler,[†] and D. N. Basov*[,†,#]

[†]Department of Physics, [‖]Department of Chemistry and Biochemistry, University of California, San Diego, La Jolla, California 92093, United States

[‡]Department of Physics, Massachusetts Institute of Technology, Cambridge, Massachusetts 02215, United States

[§]National Institute for Materials Science, Namiki 1-1, Tsukuba, Ibaraki 305-0044, Japan

[⊥]Ludwig-Maximilians-Universität and Center for Nanoscience, 80539 München, Germany

[#]Department of Physics, Columbia University, New York, New York 10027, United States

Supporting Information

ABSTRACT: We investigated phonon–polaritons in hexagonal boron nitride—a naturally hyperbolic van der Waals material—by means of the scattering-type scanning near-field optical microscopy. Real-space nanoimages we have obtained detail how the polaritons are launched when the light incident on a thin hexagonal boron nitride slab is scattered by various intrinsic and extrinsic inhomogeneities, including sample edges, metallic nanodisks deposited on its top surface, random defects, and surface impurities. The scanned tip of the near-field microscope is itself a polariton launcher whose efficiency proves to be superior to all the other types of polariton launchers we studied. Our work may inform future development of polaritonic nanodevices as well as fundamental studies of collective modes in van der Waals materials.

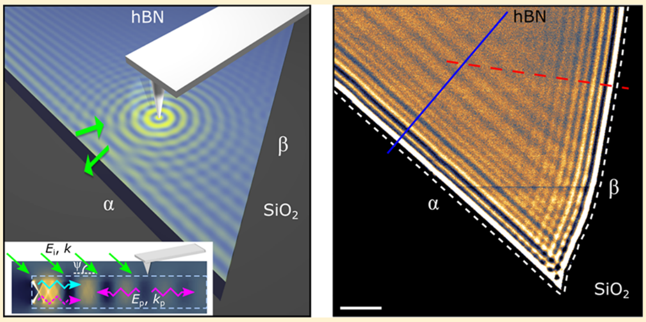

KEYWORDS: *Polariton launching, hyperbolic materials, hexagonal boron nitride, nano-optics, van der Waals materials*

Van der Waals (vdW) materials[1] have emerged as new media for the exploration of polaritons, the coupled collective oscillations of field and polarization charges.[2−4] Recently studied examples include (i) plasmon-polaritons in conductors such as graphene,[5−12] thin films of high-T_c superconductors[13] and surface states of topological insulators (TIs),[14] (ii) phonon–polaritons in insulators such as hexagonal boron nitride (hBN)[15−22] and bismuth-based TIs,[14,23] and (iii) hybrid plasmon–phonon–polariton modes in vdW heterostructures.[14,24−27] The optical permittivity of vdW materials can be extremely anisotropic, having the opposite signs along the in- and out-of-plane axes, the property known as the hyperbolic response.[28−31] Accordingly, collective modes found in these frequency ranges are referred to as the hyperbolic polaritons. Appealing characteristics of polaritons in vdW systems include high optical confinement,[5,26,32] low damping,[32] as well as exceptional mechanical, optical, and electrical tunability.[3,7,8,21,24,25,32,33]

Coupling incident light to polaritons requires overcoming their momentum mismatch.[2,3] This is possible if the system under study lacks translational invariance, for example, if the sample is of small size,[15,22] has a periodic patterning,[5,9,11] or an intrinsic inhomogeneity. Alternatively, light–polariton conversion can be facilitated by extrinsic structures brought into the sample's proximity, such as metallic stripes or plates. Such methods have been utilized for launching of plasmon polaritons in graphene.[34,35] Launching of phonon polaritons by metallic edges have been demonstrated in SiC[36] and more recently in a vdW insulator hBN.[16] Below we report on these and other types of phonon–polariton launcher in hBN and evaluate their relative efficiency. Our analysis offers guidance for the development of nano-optical systems with high-efficiency coupling to polaritonic waves.

We focus on the mid-infrared (IR) spectral range ω = 1370–1610 cm^{-1} where hBN is optically hyperbolic.[28−31] Here ω = $1/\lambda_{IR}$, and λ_{IR} is the free-space IR wavelength. The polaritons existing in this domain are referred to as the hyperbolic phonon–polaritons (HP^{2}s) since hyperbolicity in hBN

Received: April 15, 2017
Revised: July 14, 2017
Published: August 14, 2017

DOI: 10.1021/acs.nanolett.7b01587

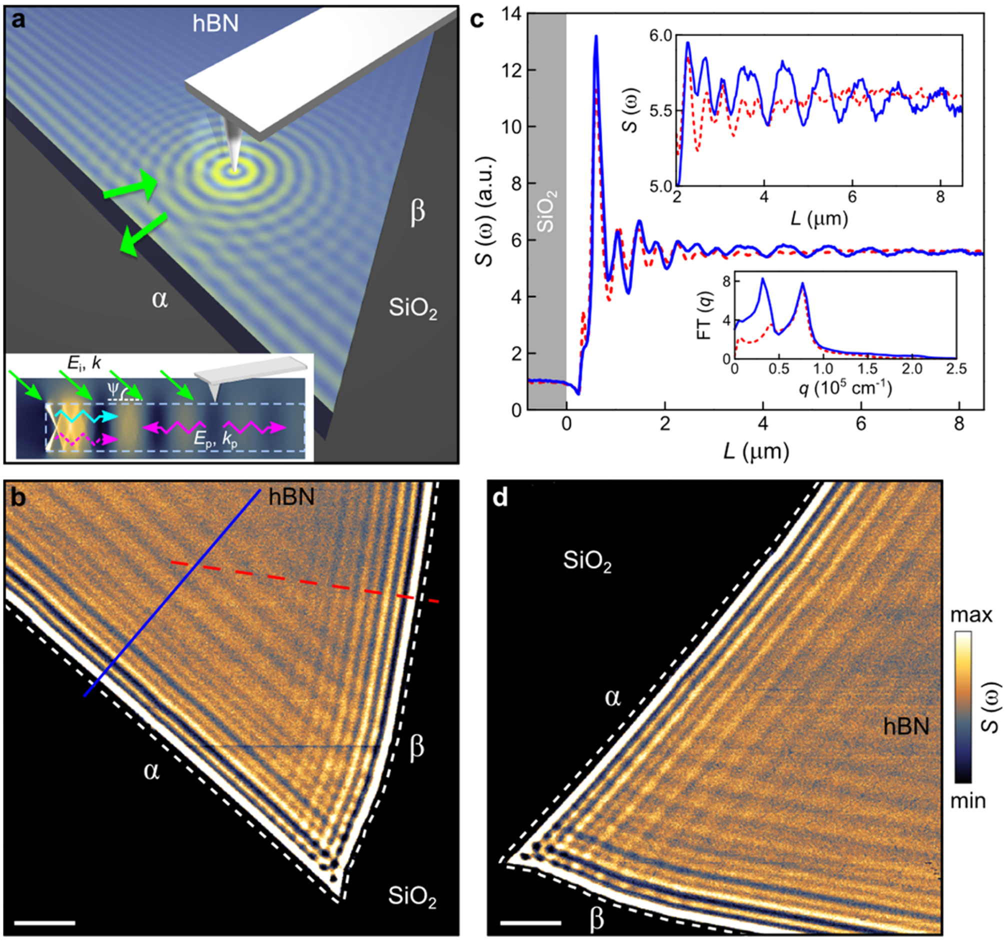

Figure 1. Polaritons launched by the s-SNOM tip and hBN edges. (a) Experimental schematic. The s-SNOM tip and a tapered hBN crystal are illuminated by the weakly focused IR beam from a quantum cascade laser (QCL). We collect the backscattered near-field signal (green arrow). Inset, the cross-section of the tip-launched (magenta arrows) and edge-launched (cyan arrow) polaritons registered by the tip. Color map, the simulation of the edge-launched polariton fringes (see Methods). (b) Near-field amplitude image of the hBN crystal in panel a. (c) Polariton line profiles taken perpendicular to the α edge (blue solid line) and β edge (red dashed line) in panel b. Insets: top, detailed view of the line profiles when $L > 2$ μm. Bottom, the Fourier transform spectra of the line profiles. (d) Near-field amplitude image of the same hBN crystal after a clockwise rotation of $\pi/2$ from panel b. White dashed lines track the hBN edges. The hBN thickness: 117 nm. IR frequency: ω = 1530 cm^{-1}. Scale bar: 2 μm.

originates from the anisotropic phonon resonances therein.[16,19,21,22,25] Real-space imaging of polaritons has been carried out using the scattering-type scanning near-field optical microscopy (s-SNOM, methods).[7,8,10,16−21,25,32] As shown schematically in Figure 1a, under the illumination of an IR laser, the polaritonic standing waves can form, and they can be visualized by scanning the sample under the tip of the atomic force microscope (AFM).[7,8,21] A representative s-SNOM image (Figure 1b) displays an oscillating pattern (or fringes) parallel to the crystal edges in a tapered hBN microcrystal. The line profile [s-SNOM amplitude $s(\omega)$ as a function of the position L along the blue line] associated with these fringes is plotted in Figure 1c. Close to the hBN edges (white dashed lines), the s-SNOM image exhibits the strongest fringe followed by several other peaks with gradually decreasing amplitude (Figure 1b−c). As established in previous studies,[17,20,21] propagating HP^{2}s waves are both launched and detected by the s-SNOM tip acting as an optical antenna.[37] These fringe patterns originate from interferences between the tip-launched (solid purple arrow) and hBN edge-reflected HP^{2}s (dashed purple arrow). The measured fringe periodicity is equal to one-half of the polariton in-plane wavelength ($\lambda_p/2$)[16,17,20,21] for the principal HP^2 branch. Interestingly, further away from the hBN edges, the $\lambda_p/2$ fringes become damped yet fringes with a much longer period persist (Figure 1b−c). These latter fringes show the period of $\sim\lambda_p$ clearly visible in the line profile (Figure 1c) and its Fourier transform (FT) (Figure 1c inset, bottom).

We attribute the origin of the period-λ_p fringes to polaritons launched by the edges of hBN crystals marked with white dashed lines in Figure 1b. The edge launching is illustrated by the annotated numerical simulation shown in the inset of Figure 1a. The green arrows in this figure represent the monochromatic IR beam, which illuminates both the hBN crystal and the s-SNOM tip. This IR beam carries the momentum $k_{IR} = 2\pi/\lambda_{IR}$ arriving at the incidence angle ψ. At the hBN edge, the IR beam excites the HP^2 wave (cyan arrow) possessing the in-plane momentum of $k_p = 2\pi/\lambda_p$. This edge-launched wave propagates away from the edge and interferes with the incident IR beam (green arrows) forming a standing wave parallel to the edge. The measured s-SNOM signal is in the first approximation proportional to the local electric field underneath the tip apex.[36] This signal is produced by the field of the IR beam E_i and that of the edge-launched polaritons E_p: $E_{tip} = E_i \cos\psi + E_p$. The period of the corresponding interference fringes is[36,38] $\delta = 2\pi/(k_p - k_{IR}\cos\psi)$. In the case of highly confined HP^{2}s in hBN,[21,22] k_p is much larger than k_{IR},

DOI: 10.1021/acs.nanolett.7b01587
Nano Lett. XXXX, XXX, XXX−XXX

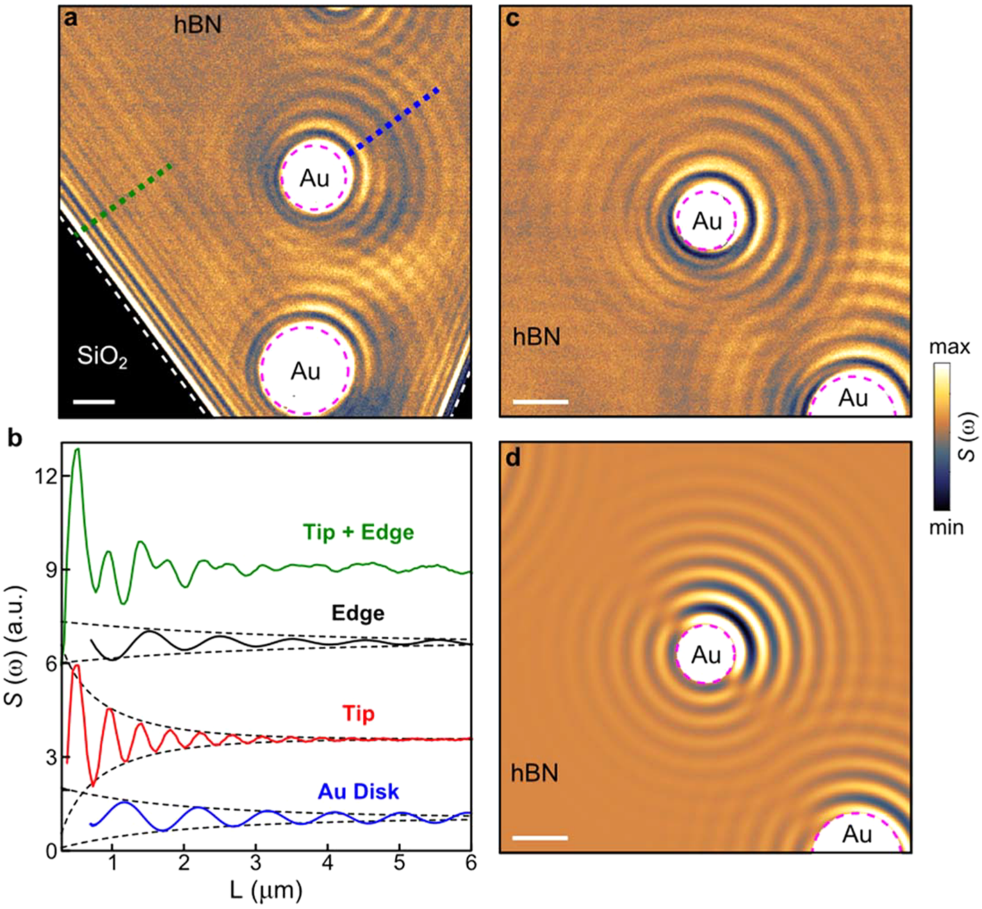

Figure 2. Polaritons launching efficiency. (a) Near-field amplitude image of the hBN crystal with artificially fabricated Au disks on top. (b) Profiles of polariton fringes as a function of the distance L from the edge of a launcher. The green and blue curves are extracted by averaging a series of linear cuts near the dotted lines in panel a. The black and red curves are obtained by the FT analysis of the green curve. The dashed curves are the fits to eq 2. (c) Near-field amplitude image of Au disks in the interior of the hBN crystal. (d) The simulation of s-SNOM image in panel c. White and magenta dashed lines track the edges of the hBN and Au disks. The hBN thickness: 117 nm. IR frequency: ω = 1530 cm^{-1}. Scale bar: 2 μm.

and so δ is close to $2\pi/\ k_p = \lambda_p$, in accordance with our data (Figures 1b–c) and numerical simulations (Figure 1a, inset). Clearly, when both edge-launched and tip-launched polaritons are present, the s-SNOM image may be rather complex. The observed pattern in Figure 1b and c is the case in point.

The different amplitudes of the λ_p and $\lambda_p/2$ polariton fringes seen in Figures 1b and d (especially in the interior of hBN) are due to their distinct propagation trajectories and travel distances (Figure 1a). Indeed, edge-launched polaritons (fringe periodicity λ_p) propagate as plane waves, whereas tip-launched polaritons ($\lambda_p/2$) propagate as circular ones. The amplitude of a circular wave decreases with the travel distance even in the absence of damping, whereas that of the plane wave does not. Furthermore, the path lengths of polaritons forming these λ_p and $\lambda_p/2$ fringes are different. The edge-launched polaritons (λ_p) only need to traverse the tip–edge distance L once to become registered in our apparatus. The tip-launched/edge-reflected polaritons (period $\lambda_p/2$) have to do a round trip. Therefore, the combination of geometric spreading and 2-fold travel distance account for the faster decrease of period-$\lambda_p/2$ oscillations in Figures 1b–c. In the interior of the hBN crystal (Figure 1b), λ_p-periodic fringes launched by the α edge (blue solid line in Figure 1c) and β edge (red dashed line in Figure 1c) exhibit different intensities. This difference is related to the shadowing of the sample by the AFM cantilever in our experiment. Once the hBN crystal is rotated by $\pi/2$, we observed identical λ_p fringe intensity (Figure 1d) from α and β edges, see Section 1 of the Supporting Information for details.

In addition to the hBN crystal edge and s-SNOM tip, polaritons in hBN are also launched by metallic nanostructures. The images in Figure 2a and c have been obtained from an hBN crystal with Au disks of height 188 nm and diameters 1–2 μm fabricated on its top surface. The s-SNOM data in Figure 2a exhibit two groups of interference fringes. The fringes in the first group are parallel to the edge; those of the other group are concentric to the Au disk. To estimate the corresponding polariton wavelengths, we examine the representative line traces (green and blue curves in Figure 2b) extracted from the s-SNOM image in Figure 2a by taking linear cuts along the lines of the same color. The green curve extracted from a line scan taken perpendicular to the hBN edge (Figure 2a) again reveals a superposition of fringes with $\lambda_p/2$ and λ_p periodicities. One can separate these components via the FT analysis.[19] In addition to the tip-launched ($\lambda_p/2$) and edge-launched (λ_p) polariton fringes (Figure 2a) parallel to the hBN edges, one can witness concentric circular fringes around the Au disks (Figure 2a and c). The profile for the concentric fringes arising from the gold launcher (blue curve, Figure 2b) exhibits oscillations with nearly the same period as the edge launched ones (black curve). Thus, it is attributed to polaritons launched by the disk edges (magenta dashed circles, Figure 2a). To verify this assertion, we numerically simulated the s-SNOM image following an earlier study[36] (Figure 2d); these simulations account for our experimental results. Note that the reflection of the tip-launched polaritons at the Au edge is weak and the $\lambda_p/2$ fringes are not evident in our data. The reason for these weak reflections is the volume-confined nature of the propagating HP^{2}s.

Let us discuss the efficiency—the ability to convert incident IR photons into propagating polaritons—of different polariton launchers. We can quantify the efficiency by taking the ratio of either the power P_p or the intensity I_p of the polariton wave to the incident IR power P_0 per unit area. The intensity scales as a square $I_p = |S|^2/M$ of the amplitude S measured by s-SNOM. The proportionality coefficient M is unknown but constant for a data set obtained for the same experimental conditions (IR frequency, illumination intensity, same tip, etc.). The ratio $l = I_p/P_0$, which has the units of length, defines the scattering length. This parameter is appropriate for an extended line-like launcher, such as an hBN edge. However, it is not suitable for a small, point-like launcher. As discussed above, such a point launcher generates waves whose intensity would decrease with distance r (measured from its center) even in the absence of damping. In the latter case, it is the total power $P_p = 2\pi r I_p(r)$ of the wave that remains constant. The proper measure of efficiency is therefore the ratio $A = P_p/P_0$, the scattering cross-section, which has the units of area. The formula for the s-SNOM amplitude, which applies to both types of launcher and includes the phase of the wave and also unavoidable damping, can be written as

$$S(r) = \sqrt{P_0 M}\, G(r) e^{i(q_p r + \phi)} \qquad (2)$$

where q_p and ϕ are the complex momentum and a phase shift, respectively. The "geometric" factor is $G(r) = \sqrt{l}$ for a line-like launcher and $G(r) = \sqrt{A/2\pi r}$ for a point-like one. Note that a metallic disk of radius $r_{disk} \gg \lambda_p$ is a type of launcher that can be considered a line-like near its edge, at $r - r_{disk} \ll r_{disk}$, and a point-like at $r \gg r_{disk}$. Accordingly, having determined its cross-section, one can also calculate the scattering length of the disk edge via $l_{disk} = A/2\pi r_{disk}$. For polaritons launched by the tip located a distance x from the edge, one should substitute $2x$, the separation between the tip and its image[7,8,21] upon reflection, for r in eq 2.

We have determined A and l by fitting the s-SNOM traces in Figure 2b to eq 2. The fits are shown by the black dashed curves. Note that all of them have the same polariton damping factor $\gamma = \mathrm{Im}\, q_p/\mathrm{Re}\, q_p = 0.055$ as in our previous studies.[19,21] For the sake of comparing *relative* efficiency, we omitted $\sqrt{P_0 M}$ in eq 2 and normalized $S(r)$ in suitable arbitrary units. From thus defined fitting procedure, we have obtained $A = 61$ (μm^2) for the s-SNOM tip, $l = 0.56$ (μm) for the hBN edge, $A = 14$ (μm^2), and $l = 1.4$ (μm) for the 1.5 μm-radius Au disk (Table 1). Note that all of these values are determined up to an unknown overall factor. We conclude that, in terms of the polariton launching efficiency, the tip is superior to the disk treated as a point-like launcher, while as a line-like launcher disk is more efficient than the edge. We attribute the higher launching efficiency of the metallic objects (the tip and the disk) to their ability to concentrate electric field—the lightning rod effect.[37] The field concentration at the hBN edge is much weaker, which explains its lower photon-to-polariton conversion efficiency. The higher launching efficiency of the tip compared to the disk indicates the former has a stronger coupling to the polaritons.[7,8,16−18,21] Note that, while r_{tip} is essentially the direct measure of s-SNOM spatial resolution, the polariton wavelength to which the tip couples most strongly is a somewhat different quantity. According to recent theory (Sec. IV of ref 39), this "optimal" polariton wavelength can be as large as $30 r_{tip} \sim 1000$ nm. In turn, the analysis presented in ref 19 indicates that the optimal coupling wavelength for a metallic disk is of the order of its diameter. Thus, the polaritons of wavelength ~820 nm seen in Figure 2 may not be too far from the optimal coupling for both the tip and the disk launchers.

Table 1. Relative Scattering Cross Sections and/or Scattering Lengths for Three Types of Launcher Studied

scattering parameter	s-SNOM tip	hBN edge	Au disk $r_{disk} = 1.5$ μm
l (μm)		0.56	1.4
A (μm^2)	61		14

One possible way to calibrate the scattering parameters A and l in absolute units is by comparison to some standard launcher for which reliable theoretical calculations are possible. The hBN edge could be a candidate for such a standard launcher provided a better understanding of the field singularities at the sharp corners is developed; see Figure 1a (inset) and Methods. This can be a subject of a future work.

Impurities and defects on the sample surface introduced unintentionally during sample fabrication (see Methods) can play the role of polariton launchers as well. As shown in Figure 3a, surface impurities (marked with magenta asterisks) act as point-like launchers that launch circular polariton waves, whereas a surface protrusion (green arrow) act as a line-like launcher. The latter one launch plane waves that do not spread much as they travel. The amplitude of these waves decays slowly and remains discernible within almost the entire field of view in Figure 3.

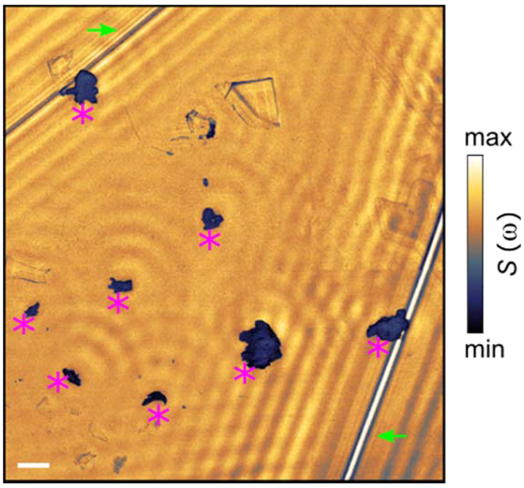

Figure 3. Near-field amplitude image of the hBN crystal with impurities (marked with magenta asterisks) and protrusion (green arrow) defect on the surface. The hBN thickness: 253 nm. IR frequency: $\omega = 1550$ cm^{-1}. Scale bar: 2 μm.

In summary, the imaging data compiled in Figures 1−3 demonstrate a variety of polariton launchers in hBN of different launching efficiency. Although essentially any topographic feature can act as a launcher, their efficiency is inferior to that of a large metalized tip. By the principle of reciprocity, the launchers studied in this work may also be employed for polariton-to-photon scattering with the resultant free-space photons detectable by conventional means. Future work may be directed toward optimizing the optical constants, size, and geometry of the polariton launchers. The methodology presented in this work may be readily extended to collective modes[2−4] in other vdW materials including graphene,[34] transition metal dichalcogenides, black phosphorus, and topological insulators. Our results along with the recent work on grating polaritonic couplers[40] present the initial steps toward developing practical polariton launchers/detectors for diverse nanophotonics applications.

Methods. *Experimental Setup.* The nanoimaging experiments described in the main text were performed at UCSD using a commercial s-SNOM (www.neaspec.com). The s-SNOM is based on a tapping-mode AFM illuminated by monochromatic quantum cascade lasers (QCLs) (www.daylightsolutions.com). These lasers cover a frequency range of 900−2300 cm^{-1} in the mid-IR. The nanoscale near-field images were registered by a pseudoheterodyne interferometric detection module with a AFM tapping frequency and amplitude around 280 kHz and 70 nm, respectively. To obtain the background-free images, the s-SNOM output signal used in this work is the scattering amplitude $s(\omega)$ demodulated at the third harmonics of the tapping frequency. The spot size of IR beam focused onto the AFM tip was 20−30 μm; therefore, the illumination of the Au and hBN crystal edges remained uniform during the scans in Figure 2b.

Sample Fabrication. Our hBN crystals were exfoliated from bulk samples synthesized with high-pressure techniques and then transferred onto Si wafers with a 300 nm thick SiO_2 layer. The Au patterns were fabricated on the hBN crystals by electron beam lithography.

Simulation of Edge-Launched Hyperbolic Phonon Polariton Fringes. The numerical simulations shown in Figure 1a (inset) were done within the quasi-static approximation. In this approach the amplitude of the scalar potential $\Phi(x, z)$ in the system is assumed to satisfy the anisotropic Laplace equation: $\partial_x(\varepsilon^x\partial_x\Phi) + \partial_z(\varepsilon^z\partial_z\Phi) = 0$, where the principal values $(\varepsilon^x, \varepsilon^z)$ of the permittivity tensor are functions of frequency ω. To produce the graphic shown in the inset of Figure 1a we used the following parameters: (1, 1) for vacuum; $(-0.5620 + 0.0678i, 2.7782 + 0.0006i)$ for hBN, and $(1.4646 + 0.0104i, 1.4646 + 0.0104i)$ for SiO_2 substrate, which are representative of frequency $\omega = 1587$ cm^{-1}. The 300 nm tall and 2050 nm wide simulation domain surrounded a 100 nm thick hBN slab. At the outer boundary of the domain the $\Phi = -x$ was imposed to model a uniform unit external field in the x-direction. This boundary-value problem was solved using MATLAB PDE Toolbox (MATLAB, Inc., Natick, MA; Release 2012b). Shown in Figure 1a (inset) are the results for the absolute value of the electric field $|E| = [(\partial_x\Phi)^2 + (\partial_z\Phi)^2]^{1/2}$. As one can see, near the corners of the hBN slab, the calculated field distribution exhibits a structure of internal criss-crossing rays, which produce “hot lines” on the surface of the slab. Further away from the edge, the calculated field distribution morphs into a gradually decaying sinusoidal wave. The internal polariton rays and the “hot lines” they produce have the same interpretation as the “hot rings” predicted in simulations and subsequently observed on sidewalls of hBN nanocones[15] and on the top surfaces of hBN slabs deposited on metallic disks.[19] Such high-intensity lines are the beats produced by coherent superpositions of multiple guided waves. As detailed in our previous work,[15,19,21] the guided waves of a slab are discrete eigenmodes characterized by the in-plane momenta $k_l = (\pi l + \chi) \tan\theta/d$, where $l = 0, 1, 2, \ldots$ is the mode number, $\chi \sim 1$ is the boundary condition dependent phase shift, and d is the slab thickness. Accordingly, the beats pattern has the periodicity $2d \tan\theta \sim \lambda_p/4$, while the parameter $\tan\theta = i\sqrt{\varepsilon^z}/\sqrt{\varepsilon^x}$ has the meaning of the slope of the polariton rays with respect to the z-axis. Unfortunately, the region where the beats exist is very narrow, and we could not probe it with our experimental resolution. On the other hand, the sinusoidal standing waves we have imaged can be identified with the principal $l = 0$ guided waves of wavelength $\lambda_p \equiv 2\pi/k_0$.

ASSOCIATED CONTENT

Supporting Information

The Supporting Information is available free of charge on the ACS Publications website at DOI: 10.1021/acs.nanolett.7b01587.

> Orientation-dependent nanoimaging data and the discussion of polariton fringe period in hBN and in graphene (PDF)

AUTHOR INFORMATION

Corresponding Author

*E-mail: db3056@columbia.edu (D.N.B.).

ORCID

Siyuan Dai: 0000-0001-7259-7182
Zhe Fei: 0000-0002-7940-5566
Yinming Shao: 0000-0002-2891-0028

Notes

The authors declare no competing financial interest.

ACKNOWLEDGMENTS

This research is supported by the ONR under grant no. N00014-15-1-2671 and the AFOSR grant no. FA9550-15-1-0478. D.N.B. is an investigator in Quantum Materials funded by the Gordon and Betty Moore Foundation’s EPiQS Initiative through grant no. GBMF4533. P.J.-H. acknowledges support from AFOSR grant number FA9550-11-1-0225 and the Packard Fellowship program.

ABBREVIATIONS

s-SNOM, scattering-type scanning near-field optical microscopy; hBN, hexagonal boron nitride; vdW, van der Waals; HP^2, hyperbolic phonon polariton; IR, infrared; AFM, atomic force microscope; FT, Fourier transform

REFERENCES

(1) Geim, A. K.; Grigorieva, I. V. *Nature* **2013**, *499* (7459), 419−425.

(2) Low, T.; Chaves, A.; Caldwell, J. D.; Kumar, A.; Fang, N. X.; Avouris, P.; Heinz, T. F.; Guinea, F.; Martin-Moreno, L.; Koppens, F. *Nat. Mater.* **2016**, *16* (2), 182−194.

(3) Basov, D. N.; Fogler, M. M.; García de Abajo, F. J. *Science* **2016**, *354* (6309), 1992.

(4) Xia, F.; Wang, H.; Xiao, D.; Dubey, M.; Ramasubramaniam, A. *Nat. Photonics* **2014**, *8* (12), 899−907.

(5) Yan, H.; Low, T.; Zhu, W.; Wu, Y.; Freitag, M.; Li, X.; Guinea, F.; Avouris, P.; Xia, F. *Nat. Photonics* **2013**, *7* (5), 394−399.

(6) Fang, Z.; Thongrattanasiri, S.; Schlather, A.; Liu, Z.; Ma, L.; Wang, Y.; Ajayan, P. M.; Nordlander, P.; Halas, N. J.; García de Abajo, F. J. *ACS Nano* **2013**, *7* (3), 2388−2395.

(7) Fei, Z.; Rodin, A. S.; Andreev, G. O.; Bao, W.; McLeod, A. S.; Wagner, M.; Zhang, L. M.; Zhao, Z.; Thiemens, M.; et al. *Nature* **2012**, *487* (7405), 82−85.

(8) Chen, J.; Badioli, M.; Alonso-Gonzalez, P.; Thongrattanasiri, S.; Huth, F.; Osmond, J.; Spasenovic, M.; Centeno, A.; Pesquera, A.; Godignon, P.; et al. *Nature* **2012**, *487* (7405), 77−81.

(9) Ju, L.; Geng, B.; Horng, J.; Girit, C.; Martin, M.; Hao, Z.; Bechtel, H. A.; Liang, X.; Zettl, A.; Shen, Y. R.; Wang, F. *Nat. Nanotechnol.* **2011**, *6* (10), 630−634.

(10) Gerber, J. A.; Berweger, S.; O'Callahan, B. T.; Raschke, M. B. *Phys. Rev. Lett.* **2014**, *113* (5), 055502.

(11) Brar, V. W.; Jang, M. S.; Sherrott, M.; Lopez, J. J.; Atwater, H. A. *Nano Lett.* **2013**, *13* (6), 2541−2547.

(12) Yang, X.; Zhai, F.; Hu, H.; Hu, D.; Liu, R.; Zhang, S.; Sun, M.; Sun, Z.; Chen, J.; Dai, Q. *Adv. Mater.* **2016**, *28* (15), 2931−2938.

(13) Stinson, H. T.; Wu, J. S.; Jiang, B. Y.; Fei, Z.; Rodin, A. S.; Chapler, B. C.; McLeod, A. S.; Castro Neto, A.; Lee, Y. S.; Fogler, M. M.; et al. *Phys. Rev. B: Condens. Matter Mater. Phys.* **2014**, *90* (1), 014502.

(14) Wu, J.-S.; Basov, D. N.; Fogler, M. M. *Phys. Rev. B: Condens. Matter Mater. Phys.* **2015**, *92* (20), 205430.

(15) Giles, A. J.; Dai, S.; Glembocki, O. J.; Kretinin, A. V.; Sun, Z.; Ellis, C. T.; Tischler, J. G.; Taniguchi, T.; Watanabe, K.; et al. *Nano Lett.* **2016**, *16* (6), 3858−3865.

(16) Yoxall, E.; Schnell, M.; Nikitin, A. Y.; Txoperena, O.; Woessner, A.; Lundeberg, M. B.; Casanova, F.; Hueso, L. E.; Koppens, F. H. L.; Hillenbrand, R. *Nat. Photonics* **2015**, *9* (10), 674−678.

(17) Shi, Z.; Bechtel, H. A.; Berweger, S.; Sun, Y.; Zeng, B.; Jin, C.; Chang, H.; Martin, M. C.; Raschke, M. B.; Wang, F. *ACS Photonics* **2015**, *2* (7), 790−796.

(18) Li, P.; Lewin, M.; Kretinin, A. V.; Caldwell, J. D.; Novoselov, K. S.; Taniguchi, T.; Watanabe, K.; Gaussmann, F.; Taubner, T. *Nat. Commun.* **2015**, *6*, 7507.

(19) Dai, S.; Ma, Q.; Andersen, T.; McLeod, A. S.; Fei, Z.; Liu, M. K.; Wagner, M.; Watanabe, K.; Taniguchi, T. *Nat. Commun.* **2015**, *6*, 6963.

(20) Xu, X. G.; Ghamsari, B. G.; Jiang, J.-H.; Gilburd, L.; Andreev, G. O.; Zhi, C.; Bando, Y.; Golberg, D.; Berini, P.; Walker, G. C. *Nat. Commun.* **2014**, *5*, 4782.

(21) Dai, S.; Fei, Z.; Ma, Q.; Rodin, A. S.; Wagner, M.; McLeod, A. S.; Liu, M. K.; Gannett, W.; Regan, W.; Watanabe, K.; et al. *Science* **2014**, *343* (6175), 1125−1129.

(22) Caldwell, J. D.; Kretinin, A. V.; Chen, Y.; Giannini, V.; Fogler, M. M.; Francescato, Y.; Ellis, C. T.; Tischler, J. G.; Woods, C. R.; Giles, A. J. *Nat. Commun.* **2014**, *5*, 5221.

(23) Talebi, N.; Ozsoy-Keskinbora, C.; Benia, H. M.; Kern, K.; Koch, C. T.; van Aken, P. A. *ACS Nano* **2016**, *10* (7), 6988−6994.

(24) Kumar, A.; Low, T.; Fung, K. H.; Avouris, P.; Fang, N. X. *Nano Lett.* **2015**, *15*, 3172.

(25) Dai, S.; Ma, Q.; Liu, M. K.; Andersen, T.; Fei, Z.; Goldflam, M. D.; Wagner, M.; Watanabe, K.; Taniguchi, T.; Thiemens, M.; et al. *Nat. Nanotechnol.* **2015**, *10* (8), 682−686.

(26) Brar, V. W.; Jang, M. S.; Sherrott, M.; Kim, S.; Lopez, J. J.; Kim, L. B.; Choi, M.; Atwater, H. *Nano Lett.* **2014**, *14* (7), 3876−3880.

(27) Huber, M. A.; Mooshammer, F.; Plankl, M.; Viti, L.; Sandner, F.; Kastner, L. Z.; Frank, T.; Fabian, J.; Vitiello, M. S.; Cocker, T. L.; Huber, R. *Nat. Nanotechnol.* **2016**, *12* (3), 207−211.

(28) Gomez-Diaz, J. S.; Alù, A. *ACS Photonics* **2016**, *3* (12), 2211−2224.

(29) Poddubny, A.; Iorsh, I.; Belov, P.; Kivshar, Y. *Nat. Photonics* **2013**, *7* (12), 948−957.

(30) Liu, Z.; Lee, H.; Xiong, Y.; Sun, C.; Zhang, X. *Science* **2007**, *315* (5819), 1686.

(31) Jacob, Z.; Alekseyev, L. V.; Narimanov, E. *Opt. Express* **2006**, *14* (18), 8247−8256.

(32) Woessner, A.; Lundeberg, M. B.; Gao, Y.; Principi, A.; Alonso-González, P.; Carrega, M.; Watanabe, K.; Taniguchi, T.; Vignale, G.; Polini, M.; et al. *Nat. Mater.* **2014**, *14* (4), 421−425.

(33) Brar, V. W.; Sherrott, M. C.; Jang, M. S.; Kim, S.; Kim, L.; Choi, M.; Sweatlock, L. A.; Atwater, H. A. *Nat. Commun.* **2015**, *6*, 7032.

(34) Alonso-González, P.; Nikitin, A. Y.; Golmar, F.; Centeno, A.; Pesquera, A.; Vélez, S.; Chen, J.; Navickaite, G.; Koppens, F.; Zurutuza, A.; et al. *Science* **2014**, *344* (6190), 1369−1373.

(35) Miscuglio, M.; Spirito, D.; Zaccaria, R. P.; Krahne, R. *ACS Photonics* **2016**, *3* (11), 2170−2175.

(36) Huber, A.; Ocelic, N.; Kazantsev, D.; Hillenbrand, R. *Appl. Phys. Lett.* **2005**, *87* (8), 081103.

(37) Atkin, J. M.; Berweger, S.; Jones, A. C.; Raschke, M. B. *Adv. Phys.* **2012**, *61* (6), 745−842.

(38) Huber, A. J.; Ocelic, N.; Hillenbrand, R. *J. Microsc.* **2008**, *229* (3), 389−395.

(39) Jiang, B.-Y.; Zhang, L. M.; Neto, A. H. C.; Basov, D. N.; Fogler, M. M. *J. Appl. Phys.* **2016**, *119* (5), 054305.

(40) Kim, S.; Jang, M. S.; Brar, V. W.; Tolstova, Y.; Mauser, K. W.; Atwater, H. A. *Nat. Commun.* **2016**, *7*, 12323.

DOI: 10.1021/acs.nanolett.7b01587
Nano Lett. XXXX, XXX, XXX−XXX

Efficiency of launching highly confined polaritons by infrared light incident on a hyperbolic material

Siyuan Dai [†], *Qiong Ma* [‡], *Yafang Yang* [‡], *Jeremy Rosenfeld* [†], *Michael D. Goldflam* [†], *Alex McLeod* [†], *Zhiyuan Sun* [†], *Trond I. Andersen* [‡], *Zhe Fei* [†], *Mengkun Liu* [†], *Yinming Shao* [†], *Kenji Watanabe*[§], *Takashi Taniguchi*[§], *Mark Thiemens*[‖], *Fritz Keilmann*[□], *Pablo Jarillo-Herrero* [‡], *Michael M. Fogler* [†], *D. N. Basov*[†Δ*].

[†] Department of Physics, University of California, San Diego, La Jolla, California 92093, USA

[‡] Department of Physics, Massachusetts Institute of Technology, Cambridge, Massachusetts 02215, USA

[§] National Institute for Materials Science, Namiki 1-1, Tsukuba, Ibaraki 305-0044, Japan

[‖] Department of Chemistry and Biochemistry, University of California, San Diego, La Jolla, California 92093, USA

[□] Ludwig-Maximilians-Universität and Center for Nanoscience, 80539 München, Germany

[Δ] Department of Physics, Columbia University, New York, New York 10027, USA

[*] Correspondence to: db3056@columbia.edu

1. Orientation-dependent nano-imaging data

The behavior of λ_p-periodic fringes (Fig. 1b of the main text) near two different edges (α and β) of the tapered hBN crystal supports their attribution to polaritons launched from the hBN edges. Indeed, these two facets of the hBN crystal are subject to different illumination conditions. As shown in Fig. 1a (main text), IR illumination of the β edge is partially blocked by the atomic force microscope (AFM) cantilever (Fig. 1a, main text), whereas the α edge is unobscured. These unequal conditions result in different amplitudes for the edge-launched polaritons, apparent from the scattering-type scanning near-field optical microscopy (s-SNOM) image (Fig. 1b) and the corresponding line profiles (Fig. 1c, main text). In the interior of hBN (Fig. 1b, main text), polaritons launched by the α edge (blue solid line) are prominent while those from the β edge (red dashed line) are much weaker (see also the line traces in the inset of Fig. 1c, top, main text). We have repeated this experiment with the hBN crystal rotated laterally by $\pi/2$, in which case the two edges experience similar infrared (IR) illumination conditions (Fig. 1d, main text, IR beam and s-SNOM tip are the same as Figs. 1a-b, main text). In this latter geometry (Fig. 1d, main text), the λ_p fringes launched by α and β edges exhibit nearly equal amplitude in the interior of hBN. The s-SNOM imaging data obtained from an hBN disk (Fig. S1) provides further evidence for the impact of AFM cantilever shadowing on polariton amplitudes. The λ_p-periodic fringes propagating at the top-right part of the disk appear weaker compared with those elsewhere due to the lower incident field in the AFM cantilever shadow.

In addition to the amplitude of the hBN edge-launched polaritons, the spatial period of these polariton fringes is also orientation-dependent (Figure S1). The period of the fringes is longer in the bottom-left region and shorter in the top-right region. As a result of the orientation-dependent oscillation period, the “focal center” (C1) of the edge-launched polariton fringes is shifted top-right from the center (C2) of the hBN disk. The physics of this varying period of the polariton fringes lies at the orientation-dependent angle between the direction of the IR illumination and that of the crystal edge[1].

2. Polariton fringe periods in hBN and in graphene

It is instructive to compare the phenomenology of the hyperbolic phonon polariton (HP^2) guided waves we have observed in hBN with that of surface plasmon polaritons (SP^2s) waves in graphene. The first generation of s-SNOM experiments were carried out with modest-quality graphene.[3,4] The imaging data obtained by these experiments were consistent with the notion of the tip-launched $\lambda_p/2$-period fringes, with λ_p being the SP^2 wavelength. More recent studies of high-quality encapsulated graphene[2, 3] have revealed fringes with the double-peak structure, implying a coexistence of $\lambda_p/2$-periodic oscillations with λ_p-period ones. Unlike the λ_p-period polariton fringes observed for hBN, those observed in graphene exhibit virtually no dependence on the in-plane polarization of the incident field[2, 4]. This latter finding indicates that the direct conversion of light into SP^2 at the graphene edge is not very important. In Ref. 1, Supplementary material, it was suggested that these longer-period fringes arise instead due to the long-range Coulomb interaction between the tip and the excess charge density induced near the edge by the tip-launched plasmon wave. Let us briefly review this argument, which was recently rediscovered in Ref. 6. Let x be the coordinate along the normal to the edge passing through the tip (such as the blue line in Fig. 1b in the main text) with the origin at the edge at $x = 0$. Far enough from the edge (s-SNOM tip position: $x = L$) the reflected wave can be described by this method of images, as a point source at $x = -L$ sending out a circular wave:

$$s(x) \propto \frac{1}{\sqrt{x+L}} e^{ik_p(x+L)+i\varphi}. \tag{S1}$$

Here $\varphi \sim 1$ is the reflection phase shift which depends on the boundary conditions. At the tip position $x = L$, the phase of the reflected wave contains the term $2k_pL$, and so the superposition of the tip-launched (purple solid arrow) and edge-reflected (purple dashed arrow) waves yields the interference fringes of period $\lambda_p/2$. Whereas Eq. (S2) describes the propagating part of the reflected wave, there should also be an evanescent part with the large-x asymptotic behavior[1]

$$s(x) \propto \frac{1}{x^a} e^{ik_pL}\,, \tag{S2}$$

where $a > 0$ is some exponent[1]. Qualitatively, one can think of the evanescent wave as composed of non-resonant polariton modes of momenta $k \sim 1/x << k_p$. Note that the phase advance of k_pL is present in both Eqs. (S1) and (S2) because the incident wave has to travel the distance L from the tip before it reaches the edge. However, there is no additional phase accumulation for the "return trip" as the evanescent wave does not oscillate. Hence, the resultant fringes have the period of λ_p, just like the polaritons directly scattered by the edge in the absence of any tip. In principle, this alternative mechanism should apply to any polariton wave governed by Coulomb interaction, including the HP^2s in hBN.

One way to discriminate between the two mechanisms of λ_p-fringes is to check the dependence of the fringe amplitude on the incident IR beam polarization. The long-range edge-tip interaction should be insensitive to in-plane component of the polarization whereas the edge-launched wave should vanish if this component is parallel to the edge. As we discussed in Section 1, in our experiment the beam-sample orientation dependence of fringes is significant. This suggests that in our hBN samples, unlike in graphene, edge-emission mechanism dominates over the long-range edge-tip interaction one. The reason for this different behavior warrants further investigation.

References

1. Huber, A. J.; Ocelic, N.; Hillenbrand, R. *Journal of Microscopy* **2008,** 229, (3), 389-395.

2. Woessner, A.; Lundeberg, M. B.; Gao, Y.; Principi, A.; Alonso-González, P.; Carrega, M.; Watanabe, K.; Taniguchi, T.; Vignale, G.; Polini, M.; et al. *Nat Mater* **2015,** 14, (4), 421-425.

3. MATLAB and Image processing toolbox Release 2012b, T. M., Inc., Natick, Massachusetts, United States. **2016**.

4. Ni, G. X.; Wang, L.; Goldflam, M. D.; Wagner, M.; Fei, Z.; McLeod, A. S.; Liu, M. K.; Keilmann, F.; Özyilmaz, B.; Castro Neto, A. H.; et al. *Nat Photon* **2016,** 10, (4), 244-247.

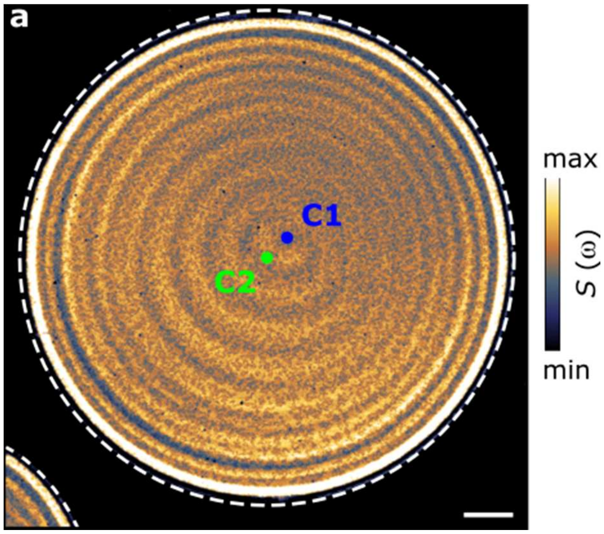

Figure S1. Polaritons in hBN disks. Near-field amplitude image of the artificially etched hBN disk. The white dashed line tracks the edge of the hBN crystal. C1 (blue) and C2 (green) indicate the "focal center" of the edge-launched polariton fringes and the geometric center of the hBN disk. The hBN thickness: 151 nm. Infrared frequency: ω = 1519 cm^{-1}. Scale bar: 2 μm.